Enhancement of Above Threshold Ionization in Resonantly Excited Helium Nanodroplets

R. Michiels[,1] M. Abu-samha[,2] L. B. Madsen[,3] M. Binz[,1] U. Bangert[,1] L. Bruder[,1] R. Duim[,1] A. Wituschek[,1]
A. C. LaForge[,4] R. J. Squibb[,5] R. Feifel[,5] C. Callegari[,6] M. Di Fraia[,6] M. Danailov[,6] M. Manfredda[,6] O. Plekan[,6]
K. C. Prince[,6] P. Rebernik[,6] M. Zangrando[,6,7] F. Stienkemeier[,1] and M. Mudrich[3,*]

[1]*Institute of Physics, University of Freiburg, 79104 Freiburg, Germany*
[2]*College of Engineering and Technology, American University of the Middle East, Egaila, Kuwait*
[3]*Department of Physics and Astronomy, Aarhus University, 8000 Aarhus C, Denmark*
[4]*Department of Physics, University of Connecticut, Storrs, Connecticut 06269, USA*
[5]*Department of Physics, University of Gothenburg, 41296 Gothenburg, Sweden*
[6]*Elettra-Sincrotrone Trieste S.C.p.A, 34149 Basovizza, Trieste, Italy*
[7]*IOM-CNR, 34149 Trieste, Italy*

Clusters and nanodroplets hold the promise of enhancing high-order nonlinear optical effects due to their high local density. However, only moderate enhancement has been demonstrated to date. Here, we report the observation of energetic electrons generated by above-threshold ionization (ATI) of helium (He) nanodroplets which are resonantly excited by ultrashort extreme ultraviolet (XUV) free-electron laser pulses and subsequently ionized by near-infrared (NIR) or near-ultraviolet (UV) pulses. The electron emission due to high-order ATI is enhanced by several orders of magnitude compared with He atoms. The crucial dependence of the ATI intensities with the number of excitations in the droplets suggests a local collective enhancement effect.

The nonlinear interaction of intense light with matter gives rise to stunning phenomena such as nonsequential double ionization [1], the emission of extreme ultraviolet (XUV) and x-ray radiation by high-order harmonic generation (HHG) [2,3], and the acceleration of electrons and ions to high energies [4,5]. In particular, HHG is widely used today for time-resolved XUV spectroscopy and attosecond science [6]. However, the conversion efficiency of HHG, usually performed in atomic gases, is notoriously low ($\lesssim 10^{-5}$). Therefore, condensed-phase targets are being explored in view of enhancing the yield and photon energy of the radiation generated by HHG.

A closely related phenomenon is the emission of electrons with kinetic energies equal to multiples of the photon energy, termed above-threshold ionization (ATI) [2]. ATI occurs when an electron absorbs more than the minimum number of photons required for ionization and manifests itself by multiple equidistant peaks in electron spectra, spaced by the photon energy. Corkum and Kulander developed a three-step semiclassical model which provides an intuitive understanding of the process leading to ATI and establishes the connection between ATI and HHG [7,8]. In this model, the radiation field lowers the potential barrier for an electron bound to an atom such that the electron may tunnel ionize. The free electron is then accelerated by the external field, and returns to the ion when the field reverses its direction. When the electron recollides with the ion, it scatters either inelastically, giving rise to HHG, or elastically, leading to high-order ATI near backward scattering. This model predicts a cutoff for the energy of emitted electrons at 10 U_p, where U_p is the electron's ponderomotive energy [9].

Previous theoretical and experimental investigations of ATI have primarily focused on atomic targets. Molecules and clusters have additional degrees of freedom such as vibration, which decrease the peak separation in the ATI electron spectra [10] and induce multiple cutoffs up to 50 U_p [11]. Using clusters, higher cutoffs were predicted as well [12,13]. The enhanced nonlinear response was discussed in the context of electron scattering from multiple centers [11,14–17]. Recently, electron-energy cutoffs far beyond 10 U_p were found for argon clusters irradiated by intense ($> 10^{14}$ W cm^{-2}) NIR and midinfrared pulses [18]. An extended rescattering model taking into account the extended potential of a multiply ionized cluster reproduced the observed scaling of cutoff energies with cluster size and the quiver amplitude of the electron in the laser field x_0. Alternatively, a macroscopic dipole moment resulting from collective oscillations of electrons about the cluster ions may lead to an enhancement of the electron energy E_e as observed in plasmonic nanostructures [19–21]. Likewise [22], clusters are promising systems for boosting HHG to higher photon energies and yields as they combine the advantage of a high local density of solids with the low average density of gases, making them dense, yet transparent, renewable targets [17,19,23,24].

In this Letter we explore the nonlinear optical response of He nanodroplets prepared in multiply excited states by irradiation with relatively intense XUV pulses. The excited nanodroplets are probed by intense near-infrared (NIR) (800 nm) and ultraviolet (UV) (400 nm) laser pulses ($\leq 3 \times 10^{13}$ W cm^{-2}) which ionize the excited He atoms, whereas the ground state He atoms in the droplets remain inactive. We find drastically extended ATI structures in the electron spectra as compared to excited He atoms in the gas phase, both for NIR and UV probe pulses. A simple semiempirical model for the collective enhancement of E_e is presented. Similar ATI spectra generated by He$^+$ ions in excited states were recently observed for strong-field ionized He nanodroplets and were used to monitor the time evolution of the nanoplasma mean-field potential [25]. In He nanodroplets doped by single foreign atoms or molecules, enhanced ATI-like electron structures were attributed to laser-assisted electron scattering upon the neutral He atoms surrounding the dopant [26,27]. In the present experiment we show indications that a collective behavior of the active atoms plays a decisive role.

In this experiment, a pulsed jet of He nanodroplets was irradiated by XUV pulses (23.7 eV) generated by the seeded free-electron laser (FEL) FERMI in Trieste, Italy [28]. At this photon energy, both the free He atoms and the He droplets are resonantly excited into the $1s4p$ state. The FEL pulses (FWHM duration 70 fs, pulse energy at the end station 2–50 nJ) were focused to an FWHM spot size of 70 μm [29]. Unless explicitly varied in the measurement, the intensity of the XUV pump pulses was $I_{\mathrm{XUV}} = 1.8 \times 10^{10}$ W cm^{-2}. At this relatively high intensity, the He droplets were multiply excited with a fraction of excited atoms ranging between 0.01% and 0.1%. The probe pulses for ionization were generated by a Ti:Sa laser (FWHM duration 100 fs) that was synchronized and collinearly superimposed with the FEL pulses. The FEL was circularly polarized, and the probe laser pulses were polarized linearly along the He jet, that is perpendicularly to the spectrometer axis. He droplets were formed in a supersonic expansion of cold He through an Even-Lavie-type pulsed valve. The mean number of He atoms per droplet, $\langle N \rangle$, was varied in the range $\langle N \rangle = 1 \times 10^3 - 7 \times 10^5$ by adjusting the temperature and opening time of the valve. The average number of excitations per droplet was controlled by $\langle N \rangle$ and the XUV intensity I_{XUV}. The He jet intersected with the laser beams at right angles inside a magnetic-bottle spectrometer mounted at the Low-Density Matter (LDM) beamline perpendicular to the He jet [30].

Figure 1 shows the typical electron spectra of He atoms (black line) and He droplets (colored lines) that are resonantly excited to the $1s4p$ state and ionized by a probe pulse at the fundamental [800 nm, (a)] or the second harmonic [400 nm, (b)] of a Ti:Sa laser synchronized with the FEL. We observe massive enhancement of the high-energy electron yield for He droplets compared with
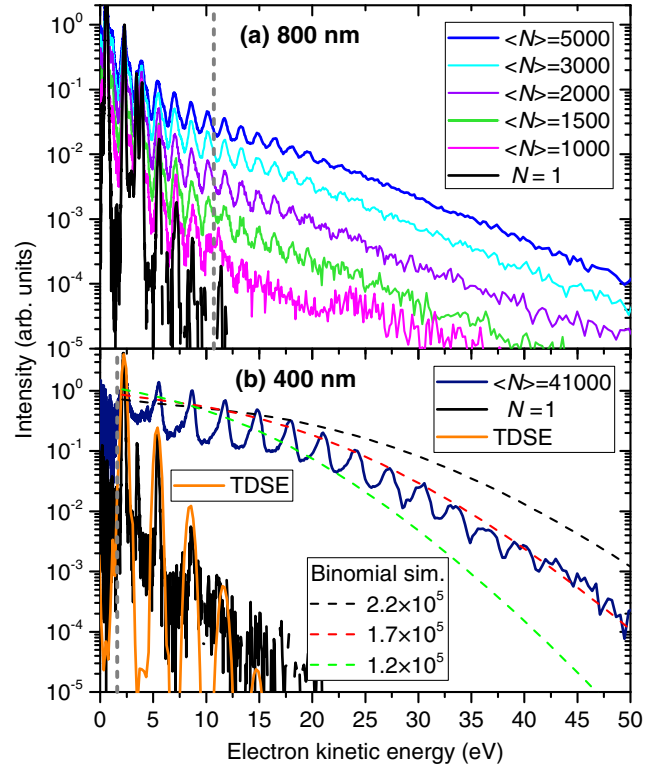

FIG. 1. Photoelectron spectra of He droplets of different mean size $\langle N \rangle$ (colored lines) compared with He atoms (black lines, $N = 1$). Both droplets and atoms are resonantly excited to the $1s4p$ state at a photon energy of 23.74 eV and ionized by NIR pulses (a) and UV pulses (b). The intensity of the probe pulses is $I_{\mathrm{NIR,UV}} \approx 10^{13}$ W cm^{-2}. The two pulses were delayed by $\tau = 4$ ps in (a) and temporally overlapped ($\tau = 0$) in (b). The vertical gray dashed lines indicate the energy $10\,U_p$. See text for discussion of the simulation curves (solid orange line for $N = 1$ and dashed colored lines for different N).

He atoms for both probe wavelengths. The enhancement is particularly pronounced at high E_e where the spectra are dominated by high-order ATI. The atomic ATI spectra are characterized by overlapping ATI peaks with exponentially decreasing intensity up to $E_e = 11$ eV (7 photons) for NIR probe pulses and 15 eV (5 photons) for UV pulses. In contrast, using droplets, ATI electrons with energies up to 150 eV are observed (see Figs. 1 and 2 in the Supplementary Material [31], which includes Refs. [32–39]).

The colored lines in Fig. 1(a) show ATI spectra recorded for different $\langle N \rangle$. At $\langle N \rangle = 1000$ (magenta curve), ATI is only weakly enhanced compared with He atoms. For larger $\langle N \rangle$, the intensity of high-order ATI continuously increases, and a plateau forms at $E_e \lesssim 25$ eV followed by an exponential drop toward higher E_e (see also Supplemental Material, Figs. 1 and 2 [31]). Figure 1(b) includes the result of a time-dependent Schrödinger equation (TDSE) calculation for He atoms in the $1s4p$ state (orange line). For details on the TDSE approach, see Ref. [40] and the Supplemental Material [31]. The good
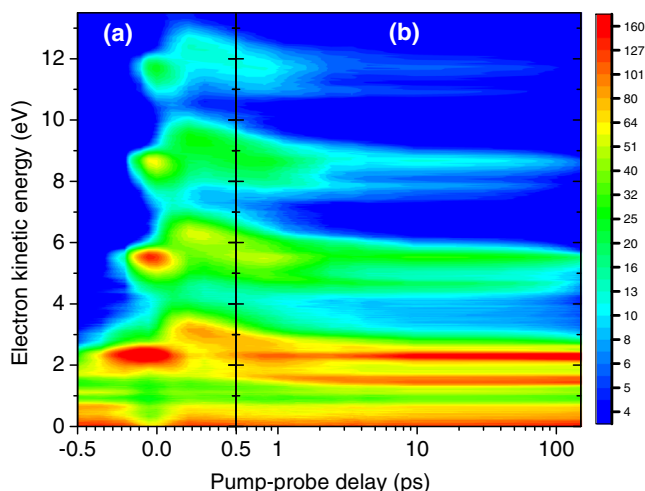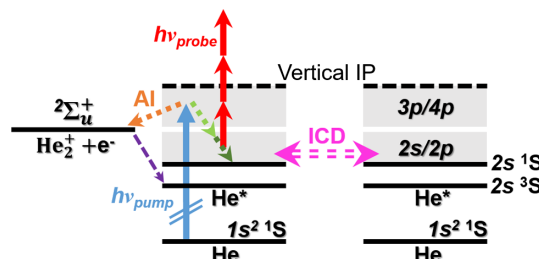
FIG. 3. Energy level diagram illustrating the competing relaxation pathways in an excited He droplet. Following resonant one-photon excitation by an XUV pump pulse, the droplet can autoionize (AI), vibronically relax into the $1s2s\,^1S$ state, or decay by ICD if a second He atom is excited nearby. Relaxation is quenched if a UV probe pulse induces multiphoton ionization shortly after the excitation.

FIG. 2. Logarithmic intensity plot of the electron spectra (vertical axis) as a function of the delay between the XUV pump and the UV probe pulses (horizontal axis). Red regions indicate high signal intensities, whereas the blue area shows the low-signal background. The short-time dynamics around zero delay is displayed in (a) on a linear scale, and the long-time dynamics is shown on a logarithmic delay scale in (b). The mean droplet size is $\langle N \rangle = 41000$.

agreement between the calculation and the experiment confirms the experimental determination of the probe-pulse intensity. Electron spectra measured for variable pump and probe-pulse intensities are shown in the Supplemental Material, Figs. 1 and 2, respectively [31].

The time evolution of the ATI spectra due to the intrinsic relaxation dynamics of He nanodroplets [41,42] is best seen for the UV probe pulses at low intensity $I_{UV} = 10^{12}$ W cm^{-2} where only a few well separated ATI peaks are present which can be examined individually. Figure 2 shows the evolution of electron spectra as a function of the pump-probe delay τ around the temporal overlap of the two laser pulses, $\tau = 0$, (a), and for large τ, (b). At $\tau = 0$, bright spots are observed at $E_e = 2.3$ eV due to $1 + 1'$ resonant pump-probe ionization of the $1s4p$-excited He droplets and at $E_e = 5.4$, 8.4, and 11.6 eV due to ATI. At $\tau \gtrsim 0.2$ ps, all ATI components spectrally broaden and slightly shift toward higher E_e. These delay-dependent changes directly reflect the dynamics of internal relaxation of the excited He nanodroplets [41–43]. The relaxation and ionization dynamics of excited He droplets is schematically illustrated in Fig. 3 and described in more detail in the Supplemental Material [31]. For longer delays [Fig. 2(b)], the low-order ATI features split in two spectral components, and the higher-order ATI lines rapidly fade away.

For a more detailed analysis, we inspect the electron spectra for selected delays τ, see Fig. 4. These spectra were recorded at even lower probe-pulse intensity $I_{UV} = 2.5 \times 10^{11}$ W cm^{-2} to allow a clear identification of the individual components. The three peaks at $\tau = 0$ (black line) exactly match the energies expected for direct

ionization of the $1s4p$-excited He droplets by $n_{ph} = 1$–3 probe photons, $E_e = 2.3$, 5.4, 8.4 eV. At $\tau = 200$ fs (red line), more than half of the population has relaxed into the $1s2s/2p$-droplet state as seen from the doubling of the peaks. The additional peaks appear shifted up in energy by 0.4 eV because the (more tightly bound) $1s2s/2p$-droplet state is now ionized by $n_{ph} = 2$–4 probe photons. At long delay ($\tau = 150$ ps), the ATI peaks nearly vanish, and the direct photoionization line splits in two ($E_e = 1.6$ and 2.2 eV) due to further relaxation into the two ^1S and ^3S spin components of the $1s2s$ He atomic state. Note that the relaxed $1s2s/2p$-droplet peaks at $\tau = 200$ fs ($E_e = 3.2$, 6.3, and 9.4 eV) still show strong ATI. Thus, the drop of the ATI intensity at $\tau \geq 200$ fs cannot be ascribed to the increase of the number of probe photons needed for
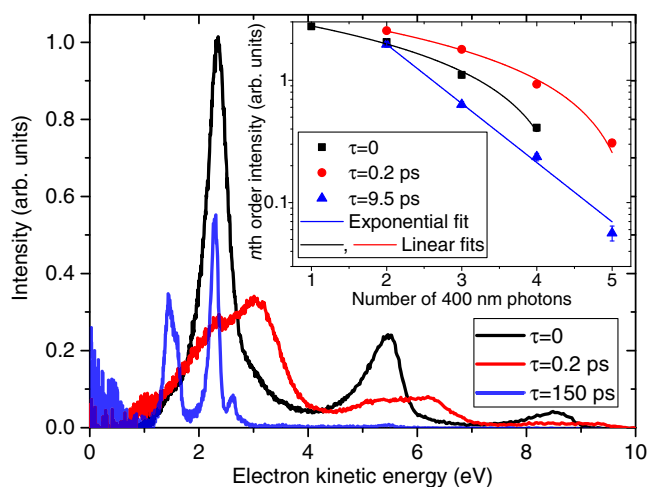

FIG. 4. Electron spectra for UV probe pulses at pump-probe delays 0, 0.2, 9.5 ps (black, red, blue lines, respectively). The spectrum recorded with only the pump pulse was subtracted to better visualize the contribution of ATI induced by the probe pulse. The inset shows on a logarithmic scale the area of the ATI peaks including linear and exponential fits. The mean droplet size is $\langle N \rangle = 41\,000$.

ionization. It is likely due to another aspect of the relaxation of excited He droplets: following the localization of the droplet excitation on excited atoms [44], the electronic relaxation is accompanied by the decoupling of He* from the droplets due to the formation of void bubbles that eventually burst at the droplet surface, thereby releasing He* into vacuum [41,42]. Clearly, ATI is enhanced in the early phase ($\tau \approx 0$) when $4p$ excitations are coupled to the droplet and delocalized, whereas ATI peaks fade away at the later stage ($\tau \geq 200$ fs) when the He* relax and detach from the droplet.

Additionally, multiple excitations in He droplets can relax by interatomic Coulombic decay (ICD) (see the pink double-sided arrow in Fig. 3 [45,46]). This nonlocal autoionization process manifests itself as a peak in the electron spectra at 16 eV, as seen in the Supplemental Material, Fig. 2, for low probe-pulse intensities. The faster decay of high-order ATI peaks compared with low orders is due to ICD being faster in droplets that contain a large number of He*.

The ATI peak areas are shown in the inset of Fig. 4 for the spectra at $\tau = 0$, 200 fs, and 9.5 ps as a function of the number of absorbed probe photons, n_{ph}. As a characteristic feature, He droplet-enhanced higher-order ATI peaks ($\tau = 0$, 0.2 ps) fall off more slowly compared with the ATI spectrum of the detached He* ($\tau = 9.5$ ps), cf. Fig. 1. The He atomic ATI intensity drops exponentially as a function of n_{ph}, whereas the droplet-enhanced ATI clearly deviates from a pure exponential decay by forming a plateaulike structure followed by an exponential drop toward higher E_e.

To quantify the He droplet-induced enhancement of ATI peaks independently of changes in the density of the He droplet jet, we consider the mean kinetic energy of the photoelectrons generated by the UV probe pulses, $\langle E_e \rangle = \int E_e \times S(E_e) dE_e / \int S(E_e) dE_e$, where $S(E_e)$ denotes the measured electron spectrum. In the atomic spectrum [Fig. 1(b)], the ATI contribution is small, and $\langle E_e \rangle$ nearly equals the energy of the $1 + 2'$ peak, $E_e = 2.23$ eV. For He droplet-enhanced ATI, we find that $\langle E_e \rangle$ strongly depends on both $\langle N \rangle$ and I_{XUV} (see Fig. 1 and Supplemental Material, Fig. 1). Therefore we consider the dependence of $\langle E_e \rangle$ on the mean number of excitations per droplet $\langle n_a \rangle = \langle N \rangle \phi_{XUV} \sigma_{2s \to 1s4p}$, shown in Fig. 5. Here, $\phi_{XUV} \propto I_{XUV}$ is the XUV photon flux per pulse and $\sigma_{1s^2 \to 1s4p}$ is the resonant absorption cross section of the $1s4p$ state. The data points are inferred from measurements performed at $I_{XUV} = 4 \times 10^8 - 1.8 \times 10^{10}$ W cm^{-2} and $\langle N \rangle = 5 \times 10^4 - 1.8 \times 10^6$. The smooth trend in the data confirms that $\langle n_a \rangle$ is the characteristic parameter determining the ATI enhancement.

A theoretical prediction of ATI in excited He nanodroplets within the existing frameworks is difficult. We observe ATI enhancement in the weak-field regime, where the quiver amplitude is small ($x_0 < 1$ Å) and $U_p \sim 10$ meV, as well as in the strong-field regime, where
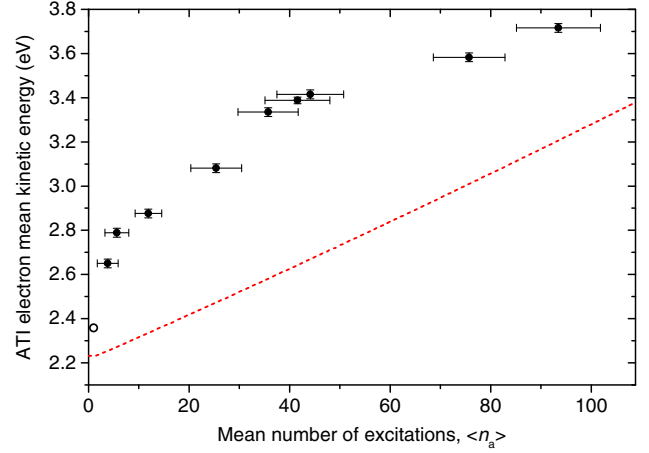

FIG. 5.   Mean electron kinetic energy as a function of the mean number of excitations per He droplet for $I_{UV} = 2.5 \times 10^{11}$ W cm^{-2}, see text. The dashed line is the result of the semiempirical model fitted to the TDSE simulation for He atoms at that value of I_{UV}. The open circle indicates the measured value for atomic He ($I_{UV} = 10^{13}$ W cm^{-2}).

$x_0 \sim 5$ Å is comparable to the mean distance between the He* in one droplet, d_{He^*}, and $U_p \sim 1$ eV. Additionally, an accurate model would require the knowledge of excited state wave functions of the He droplet. A description extending the three-step model to account for multiple scattering centers [11,14–16,18] is not applicable to our case, as even at moderate intensities (10^{12} W cm^{-2}) we see enhanced ATI, although $x_0 \ll d_{He^*}$. Plasmonic enhancement by the collective coupling of the excitations [19–21] appears better suited here, as the He* in the droplet are highly polarizable [47]. However, the polarizability of the $1s2s$ state is more than 2 orders of magnitude smaller than that of the $1s4p$ state. In Figs. 2 and 4 we observe only minor changes of the ATI enhancement when the $1s4p$ relaxes into the $n = 2$ states, thus making a crucial influence of the droplet polarization on the ATI enhancement unlikely. Laser-assisted electron scattering, as observed in doped He droplets [26], may play a role. However, the clear dependence on the number of active centers (Fig. 5 and Supplemental Material, Fig. 1) implies a different mechanism.

The model we propose here is based on the idea that the He* in a droplet interact with one another and collectively absorb photons from the probe pulse. The total absorbed energy is channeled to a single He* which emits an electron. This assumption is supported by the fact that we observe ICD at all experimental conditions in the absence of the probe pulse. The internal excitation energy of the He* does not play a role as the ATI spectra do not contain energetic electrons as in the case of ICD. Thus, the nth order of ATI is enhanced by the number of combinations resulting in the absorption of $n_{ph} + 1$ photons by an ensemble of n_a He*, given by the binomial coefficient

$$\binom{n_{\mathrm{ph}} + n_a - 1}{n_a - 1}. \qquad (1)$$

Further details are given in the Supplemental Material [31]. The shortcomings of this model are, besides its simplistic assumption of energy transfer to one electron, the neglect of the He* relaxation dynamics, the broad distribution of He droplet sizes for a given $\langle N \rangle$, and the depletion of He* due to autoionization processes [45,46]. Nevertheless, the resulting spectra reproduce the experimental data rather well [see the dashed red line in Fig. 1(b) and in the Supplemental Material, Fig. 2]. The formation of a plateau at low E_e followed by an exponential decay, as well as the shift of the cutoff toward higher E_e for increasing $\langle n_a \rangle$ is well described (Supplemental Material, Fig. 5). The dashed line in Fig. 5 shows the mean kinetic energy predicted by the model where the only adjustable parameter, an exponential decay constant obtained from a fit of the TDSE calculation for atomic He, is held constant. While the model fails to accurately match the experimental data, the overall rise of $\langle E_e \rangle$ with increasing $\langle n_a \rangle$ is reproduced. Clearly, a more rigorous theoretical treatment is needed to accurately describe the laser-driven, collective dynamics of excited states in a nanometer-sized droplet.

In conclusion, resonant multiple excitation of He nanodroplets is shown to be a route to enhancing high-order ATI far beyond the atomic ATI cutoff. The enhancement can be controlled by the number of excitations per droplet, which is determined by the droplet size and the intensity of the XUV pulse. It is limited by the relaxation of excited states which evolve into free atoms [41,42], as well as by autoionization [45,46]. Thus, the enhancement might be even more efficient for shorter pulses. Moreover, ultrashort ($\sim$10 fs), wavelength-tunable pulses would allow us to probe the role of delocalization of excitations in different states of the droplet [44]. The present study should also be extended to measuring the emission of XUV radiation from resonantly excited He nanodroplets to assess the potential of this scheme for enhancing HHG. Enhanced ATI and possibly HHG may be observed for other types of clusters as well, which can be resonantly excited by conventional laser pulses [48].

*Corresponding author.
mudrich@phys.au.dk

[1] J. B. Watson, A. Sanpera, D. G. Lappas, P. L. Knight, and K. Burnett, Phys. Rev. Lett. **78**, 1884 (1997).
[2] J. H. Eberly, J. Javanainen, and K. Rzążewski, Phys. Rep. **204**, 331 (1991).
[3] R. Ganeev, J. Mod. Opt. **59**, 409 (2012).
[4] V. Malka, S. Fritzler, E. Lefebvre, M.-M. Aleonard, F. Burgy, J.-P. Chambaret, J.-F. Chemin, K. Krushelnick, G. Malka, S. Mangles et al., Science **298**, 1596 (2002).
[5] H. Schwoerer, S. Pfotenhauer, O. Jäckel, K.-U. Amthor, B. Liesfeld, W. Ziegler, R. Sauerbrey, K. Ledingham, and T. Esirkepov, Nature (London) **439**, 445 (2006).
[6] F. Krausz and M. Ivanov, Rev. Mod. Phys. **81**, 163 (2009).
[7] J. L. Krause, K. J. Schafer, and K. C. Kulander, Phys. Rev. Lett. **68**, 3535 (1992).
[8] P. B. Corkum, Phys. Rev. Lett. **71**, 1994 (1993).
[9] G. G. Paulus, W. Becker, W. Nicklich, and H. Walther, J. Phys. B **27**, L703 (1994).
[10] J. W. J. Verschuur, L. D. Noordam, and H. B. van Linden van den Heuvell, Phys. Rev. A **40**, 4383 (1989).
[11] C. C. Chirilă and M. Lein, Phys. Rev. A **74**, 051401(R) (2006).
[12] C. Figueira de Morisson Faria, H. Schomerus, and W. Becker, Phys. Rev. A **66**, 043413 (2002).
[13] H. S. Nguyen, A. D. Bandrauk, and C. A. Ullrich, Phys. Rev. A **69**, 063415 (2004).
[14] P. Moreno, L. Plaja, and L. Roso, Europhys. Lett. **28**, 629 (1994).
[15] A. D. Bandrauk, S. Chelkowski, H. Yu, and E. Constant, Phys. Rev. A **56**, R2537 (1997).
[16] V. Veniard, R. Taieb, and A. Maquet, Phys. Rev. A **60**, 3952 (1999).
[17] J. R. V. de Aldana and L. Roso, J. Opt. Soc. Am. B **18**, 325 (2001).
[18] Z. Wang, A. Camacho Garibay, H. Park, U. Saalmann, P. Agostini, J. M. Rost, and L. F. DiMauro, Phys. Rev. Lett. **124**, 173201 (2020).
[19] J. Tisch, T. Ditmire, D. Fraser, N. Hay, M. Mason, E. Springate, J. Marangos, and M. Hutchinson, J. Phys. B **30**, L709 (1997).
[20] S. Zherebtsov, T. Fennel, J. Plenge, E. Antonsson, I. Znakovskaya, A. Wirth, O. Herrwerth, F. Süßmann, C. Peltz, I. Ahmad et al., Nat. Phys. **7**, 656 (2011).
[21] J. Passig, S. Zherebtsov, R. Irsig, M. Arbeiter, C. Peltz, S. Göde, S. Skruszewicz, K.-H. Meiwes-Broer, J. Tiggesbäumker, M. F. Kling et al., Nat. Commun. **8**, 1181 (2017).
[22] P. Fu, B. Wang, X. Li, and L. Gao, Phys. Rev. A **64**, 063401 (2001).
[23] T. D. Donnelly, T. Ditmire, K. Neuman, M. D. Perry, and R. W. Falcone, Phys. Rev. Lett. **76**, 2472 (1996).
[24] H. Park, Z. Wang, H. Xiong, S. B. Schoun, J. Xu, P. Agostini, and L. F. DiMauro, Phys. Rev. Lett. **113**, 263401 (2014).
[25] M. Kelbg, M. Zabel, B. Krebs, L. Kazak, K.-H. Meiwes-Broer, and J. Tiggesbäumker, Phys. Rev. Lett. **125**, 093202 (2020).
[26] L. Treiber, B. Thaler, P. Heim, M. Stadlhofer, R. Kanya, M. Kitzler-Zeiler, and M. Koch, Nat. Commun. **12**, 4204 (2021).
[27] B. Krebs, V. Tulsky, L. Kazak, M. Zabel, D. Bauer, and J. Tiggesbäumker, arXiv:2102.08150.
[28] E. Allaria, R. Appio, L. Badano, W. Barletta, S. Bassanese, S. Biedron, A. Borga, E. Busetto, D. Castronovo, P. Cinquegrana et al., Nat. Photonics **6**, 699 (2012).

[29] L. Raimondi, M. Manfredda, N. Mahne, D. Cocco, F. Capotondi, E. Pedersoli, M. Kiskinova, and M. Zangrando, J. Synchrotron Radiat. **26,** 1462 (2019).

[30] V. Lyamayev *et al.*, J. Phys. B **46,** 164007 (2013).

[31] See Supplemental Material at http://link.aps.org/supplemental/10.1103/PhysRevLett.127.093201 for additional experimental data, a description of the relaxation model and further details about the data analysis and modelling procedures.

[32] M. P. Ziemkiewicz, C. Bacellar, K. R. Siefermann, S. R. Leone, D. M. Neumark, and O. Gessner, J. Chem. Phys. **141,** 174306 (2014).

[33] D. S. Peterka, A. Lindinger, L. Poisson, M. Ahmed, and D. M. Neumark, Phys. Rev. Lett. **91,** 043401 (2003).

[34] D. S. Peterka, J. H. Kim, C. C. Wang, L. Poisson, and D. M. Neumark, J. Phys. Chem. A **111,** 7449 (2007).

[35] K. von Haeften, A. R. B. de Castro, M. Joppien, L. Moussavizadeh, R. von Pietrowski, and T. Möller, Phys. Rev. Lett. **78,** 4371 (1997).

[36] B. Thaler, P. Heim, L. Treiber, and M. Koch, J. Chem. Phys. **152,** 014307 (2020).

[37] M. R. Hermann and J. A. Fleck, Phys. Rev. A **38,** 6000 (1988).

[38] M. Abu-samha and L. B. Madsen, Phys. Rev. A **81,** 033416 (2010).

[39] M. Joppien, R. Karnbach, and T. Möller, Phys. Rev. Lett. **71,** 2654 (1993).

[40] T. K. Kjeldsen, L. A. A. Nikolopoulos, and L. B. Madsen, Phys. Rev. A **75,** 063427 (2007).

[41] M. Mudrich, A. LaForge, A. Ciavardini, P. O'Keeffe, C. Callegari, M. Coreno, A. Demidovich, M. Devetta, M. Di Fraia, M. Drabbels *et al.*, Nat. Commun. **11,** 112 (2020).

[42] J. D. Asmussen *et al.*, Phys. Chem. Chem. Phys. **23,** 15138 (2021).

[43] M. P. Ziemkiewicz, D. M. Neumark, and O. Gessner, Int. Rev. Phys. Chem. **34,** 239 (2015).

[44] K. D. Closser, O. Gessner, and M. Head-Gordon, J. Chem. Phys. **140,** 134306 (2014).

[45] Y. Ovcharenko, A. LaForge, B. Langbehn, O. Plekan, R. Cucini, P. Finetti, P. O'Keeffe, D. Iablonskyi, T. Nishiyama, K. Ueda *et al.*, New J. Phys. **22,** 083043 (2020).

[46] A. C. LaForge *et al.*, Phys. Rev. X **11,** 021011 (2021).

[47] Z.-C. Yan, Phys. Rev. A **62,** 052502 (2000).

[48] P. Y. Serdobintsev, A. S. Melnikov, A. A. Pastor, N. A. Timofeev, and M. A. Khodorkovskiy, J. Chem. Phys. **148,** 194301 (2018).